



Kent Academic Repository

Herklots, Jack R and Strange, Paul (2020) *Evolution of superoscillations in a relativistic wavepacket*. *Journal of Physics A: Mathematical and Theoretical*, 53 (17). pp. 175302-1. ISSN 1751-8113.

Downloaded from

<https://kar.kent.ac.uk/80659/> The University of Kent's Academic Repository KAR

The version of record is available from

<https://doi.org/10.1088/1751-8121/ab7d5f>

This document version

Author's Accepted Manuscript

DOI for this version

Licence for this version

CC BY-NC-ND (Attribution-NonCommercial-NoDerivatives)

Additional information

Versions of research works

Versions of Record

If this version is the version of record, it is the same as the published version available on the publisher's web site. Cite as the published version.

Author Accepted Manuscripts

If this document is identified as the Author Accepted Manuscript it is the version after peer review but before type setting, copy editing or publisher branding. Cite as Surname, Initial. (Year) 'Title of article'. To be published in *Title of Journal*, Volume and issue numbers [peer-reviewed accepted version]. Available at: DOI or URL (Accessed: date).

Enquiries

If you have questions about this document contact ResearchSupport@kent.ac.uk. Please include the URL of the record in KAR. If you believe that your, or a third party's rights have been compromised through this document please see our [Take Down policy](https://www.kent.ac.uk/guides/kar-the-kent-academic-repository#policies) (available from <https://www.kent.ac.uk/guides/kar-the-kent-academic-repository#policies>).

ACCEPTED MANUSCRIPT

Evolution of superoscillations in a relativistic wavepacket

To cite this article before publication: Jack R Herklots *et al* 2020 *J. Phys. A: Math. Theor.* in press <https://doi.org/10.1088/1751-8121/ab7d5f>

Manuscript version: Accepted Manuscript

Accepted Manuscript is “the version of the article accepted for publication including all changes made as a result of the peer review process, and which may also include the addition to the article by IOP Publishing of a header, an article ID, a cover sheet and/or an ‘Accepted Manuscript’ watermark, but excluding any other editing, typesetting or other changes made by IOP Publishing and/or its licensors”

This Accepted Manuscript is © 2020 IOP Publishing Ltd.

During the embargo period (the 12 month period from the publication of the Version of Record of this article), the Accepted Manuscript is fully protected by copyright and cannot be reused or reposted elsewhere.

As the Version of Record of this article is going to be / has been published on a subscription basis, this Accepted Manuscript is available for reuse under a CC BY-NC-ND 3.0 licence after the 12 month embargo period.

After the embargo period, everyone is permitted to use copy and redistribute this article for non-commercial purposes only, provided that they adhere to all the terms of the licence <https://creativecommons.org/licenses/by-nc-nd/3.0>

Although reasonable endeavours have been taken to obtain all necessary permissions from third parties to include their copyrighted content within this article, their full citation and copyright line may not be present in this Accepted Manuscript version. Before using any content from this article, please refer to the Version of Record on IOPscience once published for full citation and copyright details, as permissions will likely be required. All third party content is fully copyright protected, unless specifically stated otherwise in the figure caption in the Version of Record.

View the [article online](#) for updates and enhancements.

Evolution of Superoscillations in a Relativistic Wavepacket

J. R. Herklots and P Strange

School of Physical Sciences, University of Kent, Canterbury, Kent, CT2 7NH, UK.

(Dated: March 4, 2020)

Abstract

We analyse the evolution of superoscillations in a relativistic wavepacket. A simple superoscillating wavepacket is set up and is allowed to evolve freely according to both the Klein-Gordon equation and the Dirac equation. The superoscillations evolve anisotropically and decay after a time. Both the lifetime and anisotropy can be understood in terms of the interaction of contributions to the wavepacket from components with strongly differing complex wavenumber. The analysis is supported by numerical calculations and the results are compared with the non-relativistic analysis. A potential experiment in which the significance of relativistic effects on superoscillations could be measured is proposed.

I. INTRODUCTION:

A superoscillating function is a band-limited function that oscillates faster than its fastest Fourier component. A few decades ago, this would have been deemed impossible, such a statement initially seems paradoxical. However, such functions have been known for decades [1], but their remarkable properties only began to be realised in the late 1980's [2] and they have only been studied systematically since the mid-1990's [3]. Superoscillations are now well understood [4–14] both mathematically and physically.

Superoscillations gained the attention of experimentalists when it was also predicted that superoscillating wavepackets could be employed to image objects in sub-wavelength detail [15, 16] and there are now some impressive applications in sub-wavelength microscopy [17–19] and radar [1]. Superoscillations have even been found in a single photon [20]. The "state of the art" in our understanding of the mathematical aspects of superoscillations and their burgeoning number of applications is provided by Berry *et. al.*[21] and Chen *et. al.*[22]

In quantum mechanics Berry and Popescu [23] showed how a superoscillatory function evolves according to the free-particle Schrödinger equation. Using a prototypical superoscillatory wavepacket as the initial wavefunction, it was found that the superoscillations persist for a far longer time than expected - noticeably longer than exponentially decaying evanescent waves. This behaviour was explained through the interaction of contributions to the wavefunction appearing as complex momenta in the phase. It is this persistence of superoscillations that has been of most interest in the area of quantum superoscillations with the case of the harmonic oscillator [24, 25], a uniform electric field [14] and a uniform magnetic field [26] all being studied. In these cases it is found that superoscillations behave in much the same way as they do for free particles, although in the harmonic oscillator potential they re-form periodically. For the case of the electric field, it is found that the superoscillations disappear on a time scale identical to that of the free-particle. However, in this interpretation and others [14] a more general Hamiltonian was used and, consequently, it was found that the time for which superoscillations exist is dependent on the initial wavevector (actually N in the subsequent theory).

In the end nature is governed by relativistic physics, not non-relativistic physics and these previous studies all contain the inherent approximation of being non-relativistic. While this is true of all non-relativistic theory, in the case of superoscillations it is particularly salient

1
2
3 because they are exponentially small and relativistic effects may well be of the same order
4 of magnitude as the superoscillations themselves. Any experimental predictions or physical
5 applications based on the work of Berry and Popescu have an unknown limitation for this
6 reason. In the present paper we remove this approximation to address the question of how
7 relativity affects the formation, behaviour and decay of superoscillations within quantum
8 theory. In principle this deepens our understanding of the subject and provides a more
9 realistic understanding of the theoretical limits of many of the above applications.
10
11
12
13
14
15
16
17

18 One way in which superoscillations can be probed was suggested by Berry and Popescu[23].
19 Because their wavefunction $\psi(x)$ is periodic it can represent a grating that transforms an
20 incident plane of quantum particles into a propagating series of diffracted beams. For
21 incident light such a grating could be manufactured by programming a spatial light mod-
22 ulator. If the relativistic theory can be fully understood and an analogous "grating" can
23 be manufactured for particles it could be used to create particle beams which can be used
24 to measure relativistic effects on superoscillations directly. These beams will also have
25 unusual cross sectional profiles for further experiments and applications. We examine how
26 superoscillations evolve in relativistic single particle quantum mechanics by considering in
27 detail a simple superoscillating wavepacket and comparing our results with those derived
28 from the Schrödinger equation. There is no reason to believe that the wave packet we have
29 chosen is not typical of any superoscillating wavepacket.
30
31
32
33
34
35
36
37
38
39
40
41

42 The paper is laid out as follows. In the following section we introduce and discuss the
43 elementary properties of our wavepacket. Then in section III we discuss an initial wave packet
44 of this form that is allowed to evolve as a relativistic spin-0 particle according to the Klein-
45 Gordon equation. In the following section we examine the evolution for a spin-1/2 particle
46 and show that if the Dirac equation is written in a convenient representation the solutions
47 of the Klein-Gordon equation can be used to deduce the behaviour of all components of
48 the Dirac wavefunction. Finally we compare the results from both relativistic wave packets
49 and draw some conclusions about relativistic effects on superoscillating behaviour. Because
50 they are rarely discussed we also provide an appendix discussing relativistic first quantised
51 propagators.
52
53
54
55
56
57
58
59
60

II. SUPEROSCILLATIONS

Following Berry and Popescu we consider the wavepacket

$$\psi(x, 0) = (\cos(x) + ia \sin(x))^{\mathcal{N}} \quad (1)$$

where $a > 1$ is a number, and \mathcal{N} is large. $\psi(x, 0)$ is a repeating function with period 2π . Obviously for $a = 1$ it is a simple plane wave. The properties of this wavepacket have been considered in detail by Aharonov and co-workers [4]. Close to $x = 0$ we can write $\psi(x, 0)$ as

$$\psi(x, 0) = \exp(\mathcal{N} \log(1 + iax)) \approx \exp(ia\mathcal{N}x) \quad (2)$$

which is a simple plane wave with effective wave vector $a\mathcal{N}$. In [23] Berry and Popescu evaluated the Fourier series for $\psi(x, 0)$ and found

$$\psi(x, 0) = \sum_{n=0}^{\mathcal{N}} c_n \exp(i\mathcal{N}\kappa_n x) \quad (3)$$

with

$$\kappa_n = 1 - \frac{2n}{\mathcal{N}} \quad c_n = (-1)^n \frac{(\mathcal{N})!}{2^{\mathcal{N}}} \frac{(a^2 - 1)^{\mathcal{N}/2}}{[\mathcal{N}(1 + \kappa_n)/2]![\mathcal{N}(1 - \kappa_n)/2]!} \left(\frac{a-1}{a+1}\right)^{\mathcal{N}\kappa_n/2} \quad (4)$$

which is band-limited, containing only wavenumbers $|\kappa_n| \leq 1$. Equation (2) can oscillate arbitrarily more rapidly than equation (3) (depending on the value of a) and so this function is described as superoscillating.

In Figure 1 we show $\psi(x, 0)$ for $\mathcal{N} = 20$ and $a = 4$. The superoscillations occur close to $x = 0$ where the wavepacket is flat in this figure. This is representative of a general property of superoscillating wavepackets. Superoscillations occur in regions of space where the amplitude of the wave is exponentially small. The question that then arises is how to display superoscillations in a way that enables them to be observed. We do this by plotting the logarithm of the real part of the wavepacket, the imaginary part behaves similarly. Then, because $\log 0 = -\infty$, the nodes of the wavefunction are easily seen.

III. SPIN-0 WAVEPACKETS

A. The Klein-Gordon equation

In relativistic quantum theory spin-zero particles are described by the Klein-Gordon equation [27] and it is this case we focus upon. We will consider free particles in 1+1

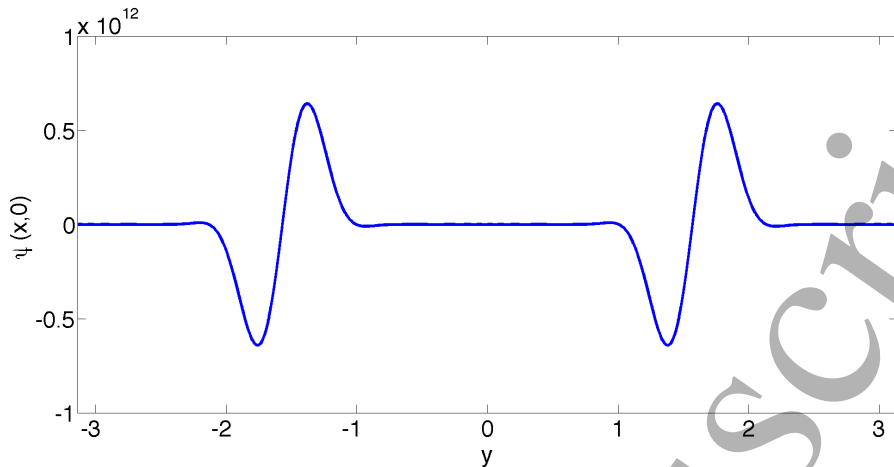


FIG. 1. The wavepacket described by equation (1) for $\mathcal{N} = 20$, $a = 4$ and $k = 1$. The flat region centred on the origin is where the superoscillations exist.

dimensions only and this equation then takes the form

$$\left(-\frac{1}{c^2} \frac{\partial^2}{\partial t^2} + \frac{\partial^2}{\partial x^2}\right) \psi(x, t) = N^2 c^2 \psi(x, t). \quad (5)$$

In general the solutions to this can be written in terms of plane waves

$$\psi(x, t) = \sum_n A_n \exp(i(k_n x - \omega_n t)) \quad (6)$$

with

$$\omega_n^2 = k_n^2 c^2 + N^2 c^4. \quad (7)$$

In these equations we have replaced m/\hbar by N in the usual form of the Klein-Gordon equation. This is convenient because later on Nc will be assumed to be large. We can take the linear combination in equation (6) corresponding to the wavepacket of equation (1) at $t = 0$. That means we identify A_n with c_n , $k_n = \mathcal{N}\kappa_n$ and $\mathcal{N} = Ncs$ where s is a constant with spatial dimensions and magnitude $1/c$, which is required for the dimensions to make sense. It will be seen later that s does have a significant role to play in the evolution of superoscillations in this wavepacket. It is then clear that the solutions at all times are

$$\psi(x, t) = \sum_{m=0}^N c_n \exp(iNcsk_n x - \omega_n t) \quad (8)$$

$$\omega_n^2 = N^2 k_n^2 s^2 c^4 + N^2 c^4 \quad (9)$$

In Figure 2 we display the superoscillations as a function of position for a series of increasing times. Figure 2a is for $t = 0$ and shows the superoscillations in the central region of figure 1. The graphs in Figure 2 have been evaluated at the same times as those in Figure 4 of reference [23]. Comparison of their figure with ours shows that the figures are broadly similar, but differ substantially in detail. In particular we note that the figures rapidly lose their symmetry. In 2c and 2d for example, the wavepacket hardly passes through zero at all for $x < 0$ while it does so frequently for $x > 0$. This suppression of superoscillations on one side of the origin was termed "the wall effect" by Berry and Popescu [7]. We can also see from this figure that by time $t = \pi/2$ the super oscillations have disappeared. To better view the evolution of superoscillations and see the effects of relativity we plot a

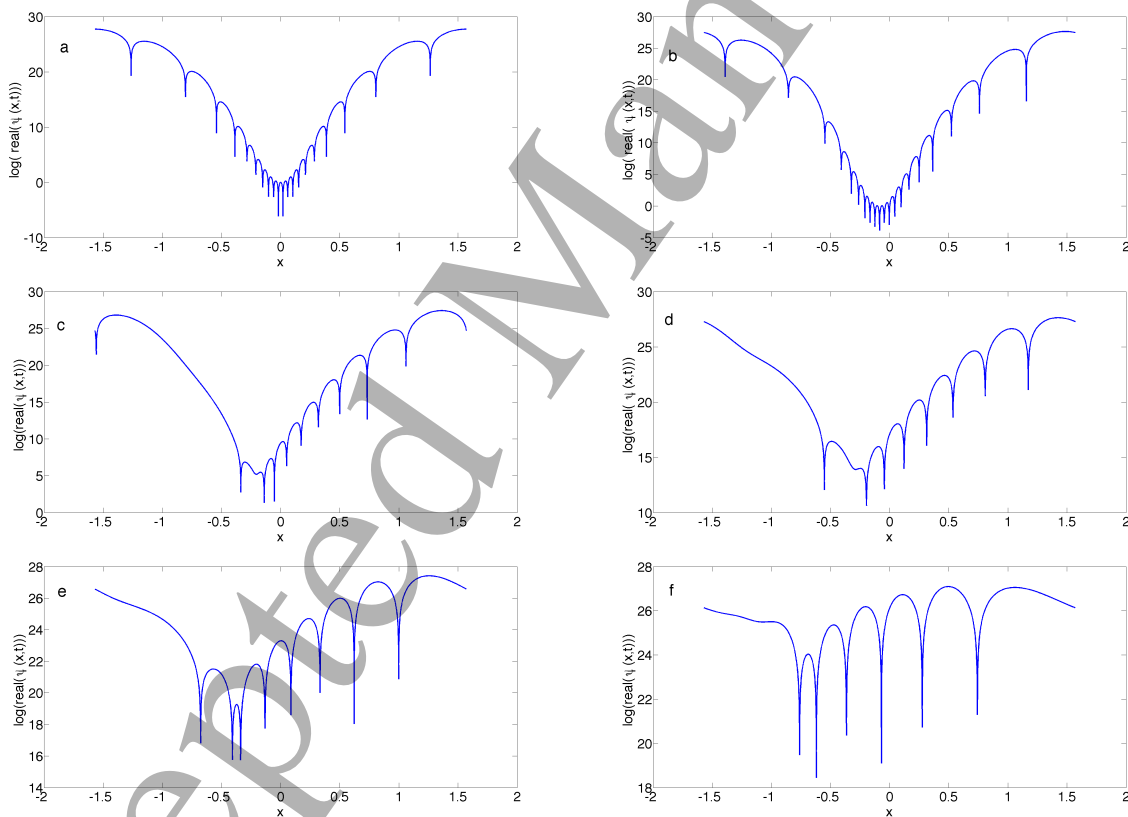


FIG. 2. The logarithm of the real part of the wavepacket described by equation (8) for $\mathcal{N} = 20$, $a = 4$ and $c = 2$ at a series of times: a) $t = 0$; b) $t = 0.015\pi$; c) $t = 0.08\pi$; d) $t = 0.706$; e) $t = \pi/2$; f) $t = \pi$.

space-time map of the density $\log(\Re(\psi(x,t)))$ in Figure 3. In this figure we have removed the rest mass frequency Nc^2 from ω to make direct comparison with the non-relativistic case.

1
2
3 It should be noted that the white lines (the wavefunction zeroes) are the only physically
4 significant quantity on these figures. The greyscale has a normalisation dependence which
5 is not necessarily identical in each figure. Figures 3a and b show the non-relativistic limit
6 of our code taken by setting $c = 50$ and presented on two different scales. Comparison
7 with Figure 3 of the paper by Berry and Popescu shows that the lines are identical apart
8 from an unimportant inversion about $x = 0$ which we cannot explain. There is an apparent
9 rescaling, but this is simply due to the relativistic units we have employed. Figures 3 c and d
10 show the superoscillations when we emphasise relativistic effects more by setting $c = 2$ and
11 figures 3 d and e are for when $c = 1$. In this paper we wish to emphasise relativistic effects
12 and the usual way to do this would be to set $c = 1$. If we do that in this case the kinetic
13 energy of the highest Fourier component is equal to Nc^2 and we would have to consider
14 particle/antiparticle creation. Therefore we have set $c = 2$ throughout the rest of this paper
15 which means the kinetic energy is still a large fraction of the rest mass energy, but well
16 below it, so we can ignore particle/antiparticle creation and the one-particle approach is an
17 excellent approximation.
18
19
20
21
22
23
24
25
26
27
28
29
30
31
32
33
34

35 Displaying superoscillations using the logarithm of the real part of the wavefunction
36 means we are displaying its phase. Subtracting the rest mass energy changes the phase and
37 so our results depend on this. To display this explicitly we present figure 4 where we show
38 the evolution of superoscillations for when the rest mass energy is removed from the total
39 and the full relativistic case where it is included. Clearly the results are very different and
40 Figure 4a is the correct one to compare with the non-relativistic limit while Figure 4b is
41 the one that is more correct within a fully relativistic theory. Henceforth we will display
42 superoscillations with the full relativistic energy.
43
44
45
46
47
48
49
50
51
52
53

54 While Figures 3 and 4 are informative we can gain little insight into the reasons for the
55 wall effect and the disappearance of super oscillations from them. To make further progress
56 we examine the wavefunction as a function of time using a propagator approach.
57
58
59
60

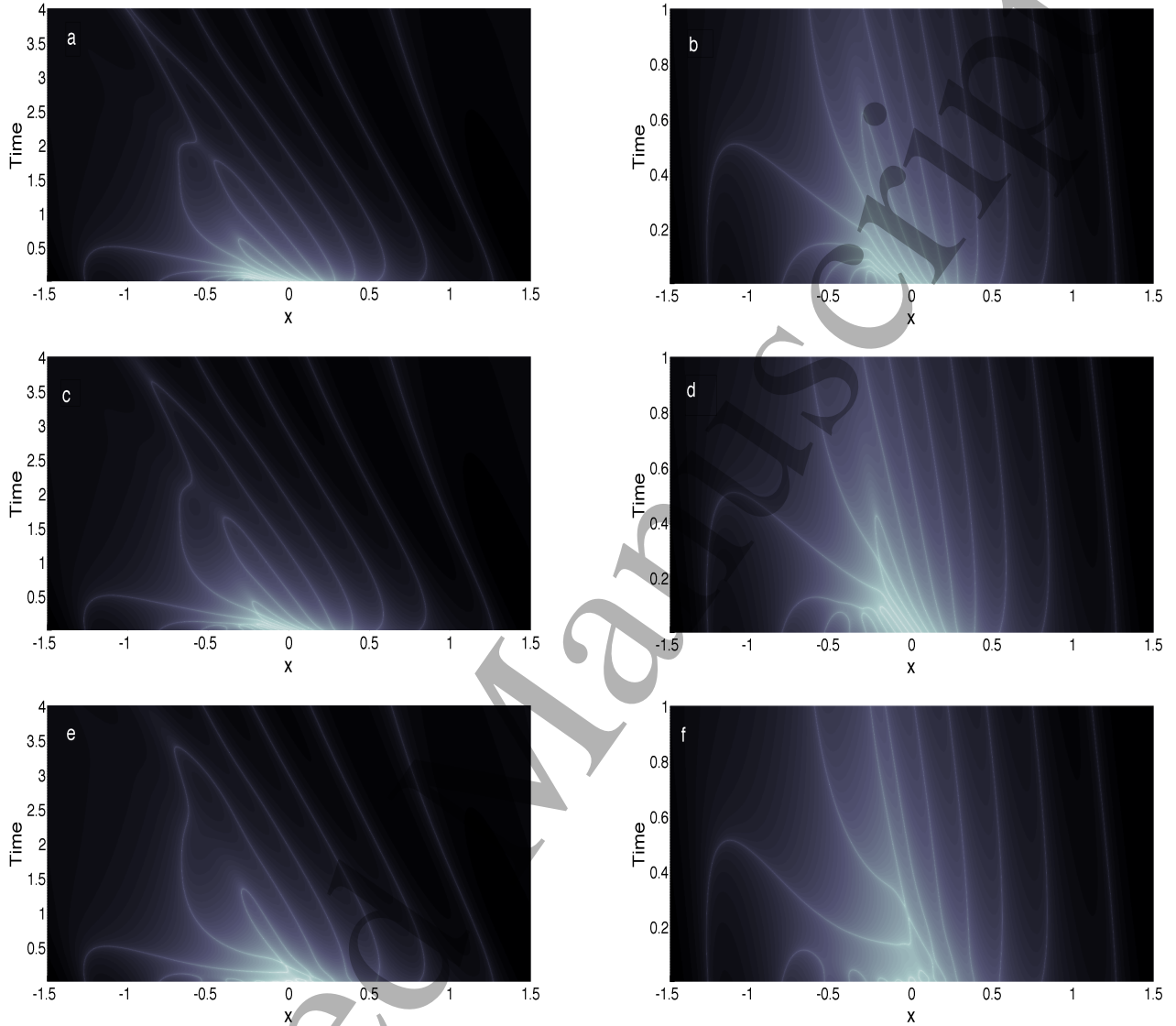


FIG. 3. Density maps for $\log \Re(\psi(x, t))$ on a large (left column) and more detailed (right column) scale for a wavepacket with $a = 4$ and $N = 20$. a and b for $c = 50$ (the non-relativistic limit), c and d for $c = 2$ (the relativistic case) e and f for $c = 1$ (the strongly relativistic case)

B. Quantum Evolution in terms of the Relativistic Propagator

The Klein-Gordon propagator is derived in the appendix. To gain a deeper understanding we write the wavefunction in the propagator representation

$$\begin{aligned} \psi(x, t) &= \int_{-\infty}^{\infty} \psi(x', 0) \Delta(x - x', t) dx' \\ &= \frac{A}{\sqrt{L}} \frac{iN}{\pi} c^2 t \int_{-\infty}^{\infty} (\cos kx' + ia \sin kx')^{Ncs} \frac{K_1(Nc\sqrt{(x-x')^2 - c^2t^2})}{\sqrt{(x-x')^2 - c^2t^2}} dx' \end{aligned} \quad (10)$$

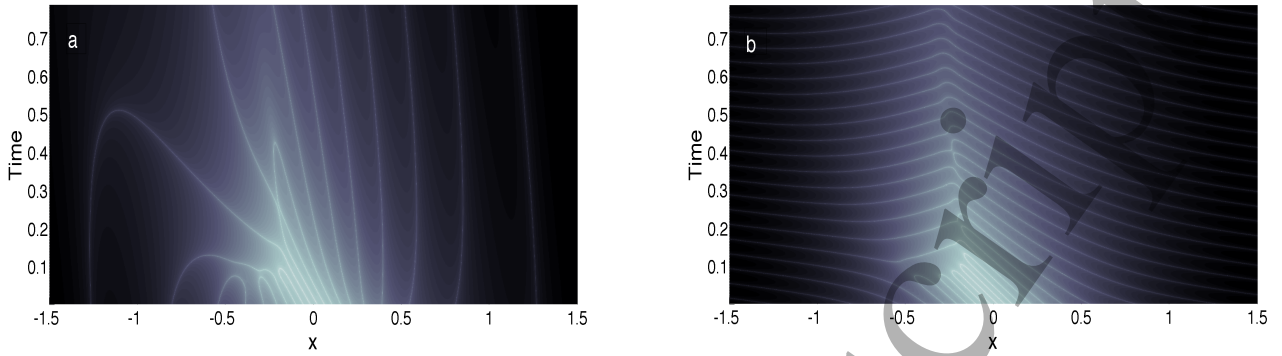


FIG. 4. Density maps for $\log \Re(\psi(x, t))$ for a wavepacket with $a = 4$ and $N = 20$. a) Calculated with the rest mass subtracted from the total relativistic energy; b) calculated with the full relativistic energy.

where A is the normalisation constant and L is the normalisation length. We have also introduced a simple wave vector k to give us control over the scale of the problem and to simplify the units. The integrand here is a complex function containing saddle points plus poles at $x' = x \pm ct$. We now consider evaluating this integral at various levels of approximation.

1. The Poles

To take account of the contribution to the integral from the poles at $x' = x \pm ct$ we make the light cone approximation to the propagator. This is given by equation (28). Putting this into equation (10), separating into partial fractions and retaining only positive times yields

$$\begin{aligned} \psi(x, t) &= -\frac{iA}{2\pi\sqrt{L}} \int_{-\infty}^{\infty} \frac{(\cos kx' + ia \sin kx')^{Ncs}}{x - x' + ct} dx' \\ &= -\frac{iA}{2\pi\sqrt{L}} \sum_{m=0}^{Ncs} c_m \int_{-\infty}^{\infty} \frac{e^{iNcsk_mx'}}{x - x' + ct} dx' \end{aligned} \quad (11)$$

where in the final step we have replaced the explicit form of the wavepacket by its Fourier decomposition. This integral can be evaluated using the residue theorem. However care must be taken when deforming the contour. The terms with negative k_m diverge as $x' \rightarrow +i\infty$ and the terms with positive k_m diverge as $x' \rightarrow -i\infty$. When $k_m = 0$ the integral is convergent and which contour is selected doesn't matter. The contours chosen are shown in Figure 5.

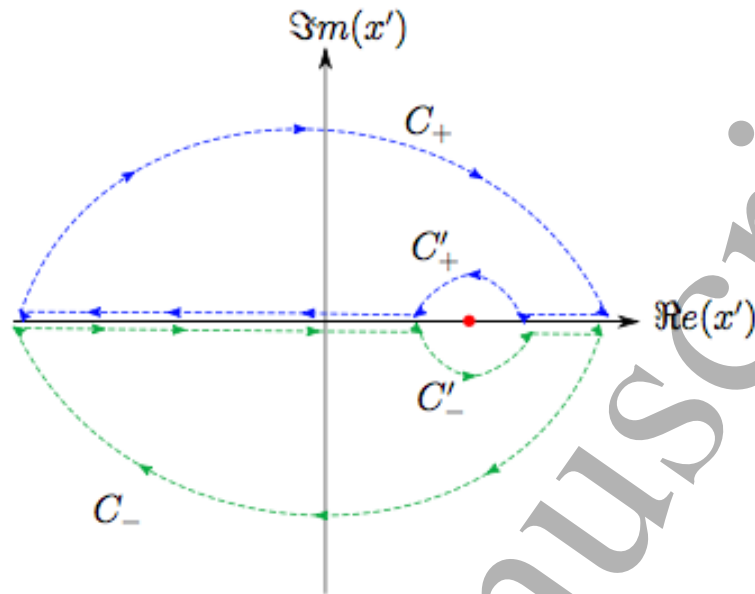


FIG. 5. This figure shows how the sign of k_m in equation (11) affects how the contour is deformed around the pole (red circle) at $x' = x + ct$ in the x' plane. If $k_M > 0$ the contour is deformed to C_+ and if $k_m < 0$ it is deformed to C_- .

Taking all this into account a trivial calculation then yields

$$\psi(x, t) = \frac{A}{\sqrt{L}} (\cos(k(x + ct)) + ia \sin(k(x + ct)))^{Ncs} \quad (12)$$

This turns out to be a very poor approximation to the full wavefunction after $t = 0$ and cannot tell us anything about superoscillations. This is because the light cone approximation propagates the initial wavefunction at the speed of light whereas the actual evolution involves the interference of $2N+1$ plane waves all travelling at different speeds.

2. The Saddle Points

In order to get an expression that is integrable the following representation of the initial wavefunction is used

$$\psi(x, 0) = \frac{A}{\sqrt{L}} (\cos kx + ia \sin kx)^{Ncs} = \frac{A}{\sqrt{L}} \exp \left[iNcs \int_0^x q(x'') dx'' \right] \quad (13)$$

where $q(x)$ is an effective local complex wavevector (momentum) given by

$$q(x) = -i \frac{\partial}{\partial x} \log (\cos kx + ia \sin kx) = \frac{ak \cos kx + ik \sin kx}{\cos kx + ia \sin kx} \quad (14)$$

The wavefunction in this representation is then given by

$$\psi(x, t) = \frac{iA}{\sqrt{L}} ct \sqrt{\frac{Nc}{2\pi}} \int_{-\infty}^{\infty} \frac{\exp\left(Nc(is \int_0^{x'} q(x'') dx'' - \sqrt{(x-x')^2 - c^2 t^2})\right)}{((x-x')^2 - c^2 t^2)^{3/4}} dx' \quad (15)$$

where we have used equation (29) for the propagator. Now Nc can be taken as a large parameter and this integral can, in principle, be done using the saddle point method. The phase of the exponential is defined as

$$\phi(x'; x, t) = is \int_0^{x'} q(x'') dx'' - \sqrt{(x-x')^2 - c^2 t^2} \quad (16)$$

Differentiating the phase and setting the result equal to zero gives the saddle point condition

$$q(x_j) = \frac{i(x-x_j)}{s\sqrt{(x-x_j)^2 - c^2 t^2}} \quad (17)$$

where x_j are the values of x' at which equation (17) is valid. Interestingly the saddle points occur at values of x' at which the complex wavevector is equal to the derivative of the space-time interval multiplied by i/s . Equation (15) is still not easy to evaluate because the periodic nature of $q(x)$ means there is an infinite number of saddle points. As in the non-relativistic case, superoscillations occur at low values of x and t so it suffices to make a small x approximation to equation (13) and (14).

$$\begin{aligned} \psi(x, 0) &= \frac{A}{\sqrt{L}} (1 + iakx)^{Ncs} \\ q(x) &= \frac{ak}{1 + iakx} \end{aligned} \quad (18)$$

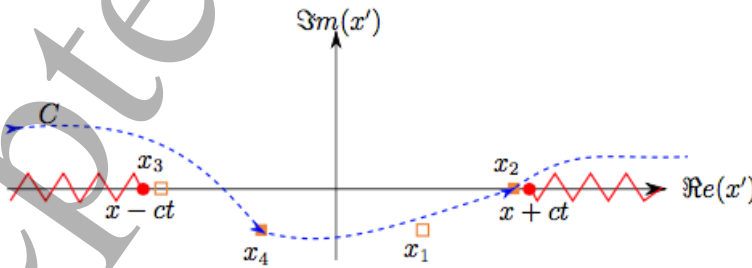


FIG. 6. The complex plane in which the integration contour C is deformed through the saddle points at x_2 and x_4 . The branch cut emanating from the branch points at $x' = x \pm ct$ is shown in red.

If we substitute this equation for $q(x)$ into equation (17) we obtain a quartic equation for four saddle points. This has been solved this using the *roots* subroutine in Matlab. There are

four saddle points two moving forwards in time corresponding to positive energy particles and two moving backwards corresponding to negative energy particles. In order to get a wavefunction of purely positive energy only the saddle points corresponding to time moving forward are considered. It has been found numerically that these are the saddle points at x_2 and x_4 shown in figure 6, and the figure also displays how the contour is deformed to pass through them. Once the saddle points and the contour have been established it is straightforward [31, 32] to find an approximate value of the integral in equation (15).

$$\psi(x, t) \approx ict \sum_j \sqrt{\frac{-A}{L\phi''(x_j; x, t)}} \frac{\exp[Nc\phi(x_j; x, t)]}{((x - x_j)^2 - c^2t^2)^{3/4}} \quad (19)$$

where the sum is over contributions from both time-forward saddles. In Figure 7 we show

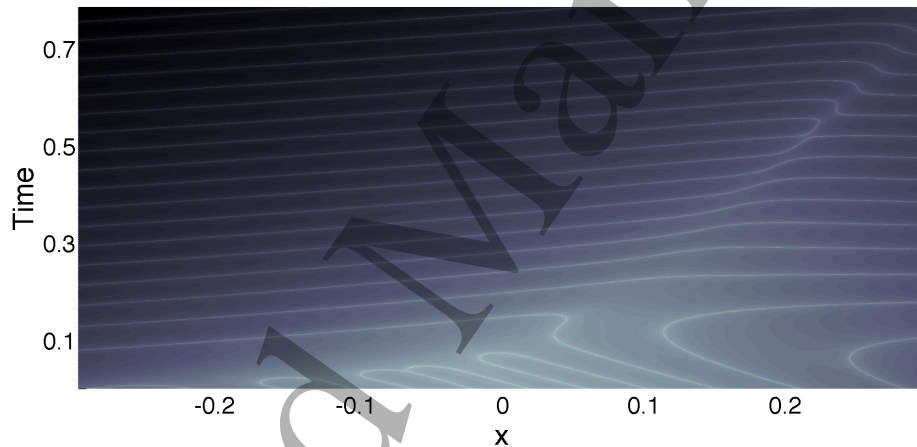


FIG. 7. Density maps for $\log \Re(\psi(x, t))$ for a wavepacket with $a = 4$ and $N = 20$ calculated using the propagator and the full relativistic energy.

the superoscillations not far from $(x, t) = (0, 0)$ calculated from equation (19). As explained earlier we plot the superoscillations with the rest mass included in the calculation of the energy in Figure 7. Clearly they resemble the exact superoscillations shown in figure 4b at low values of x and t but vary from this increasingly as x and t increase. In truth there are small differences even at low values of x and t , but the gross behaviour we wish to examine is still evident. For example in Figure 4b an approximately vertical line can be discerned where the behaviour of the waves changes. The same line exists, but is less visible in Figure 4a. These lines can also be seen in Figures 7, but now move slowly to more positive x as time increases.

At a general point the contribution of the saddles to the total in equation (19) will be exponentially different. There are regions where the x_2 saddle dominates the one at x_4 and vice versa. These regions are separated by anti-Stokes lines where the absolute values of the exponentials in equation (19) are equal. Figure 8 shows the contribution of each saddle point to the total integral in equation (19). We note that there is one discontinuous zero in Figure 8b. This is due to $\phi''(x_j : x, t)$ passing through zero and the saddle point method is invalid close to this point.

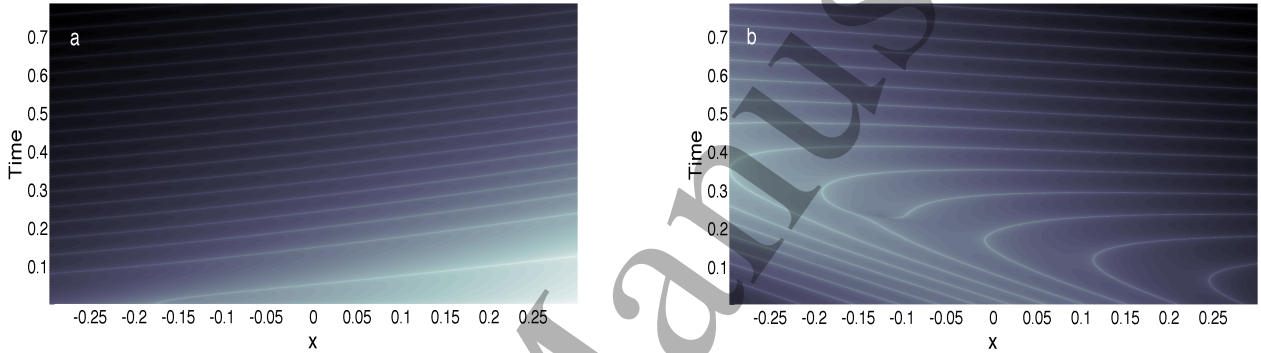


FIG. 8. Density maps for $\log \Re(\psi(x, t))$ for a wavepacket with $a = 4$ and $N = 20$ calculated using the propagator. a) Calculated for the saddle at x_4 ; b) calculated for the saddle at x_2 .

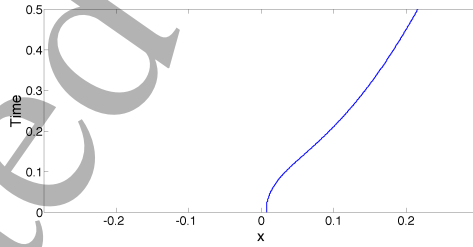


FIG. 9. The AntiStokes line which divides space into a regions where the wavefunction is dominated by the contribution from the saddle at x_2 (to the right of the AntiStokes line) and a region where it is dominated by x_4 (to the left of the AntiStokes line) .

If we now compare Figure 8 with Figure 7 we see that on the left and towards the top of Figure 7a the superoscillations are dominated by the saddle at x_4 while on the lower right they are dominated by the saddle at x_2 . Luckily the place where the saddle point method is invalid for calculating the contribution from x_2 is well inside the regions dominated by the saddle point at x_4 and so it does not affect our discussion. In Figure 9 we plot the

1
 2
 3 anti-Stokes line which comes down to close to the origin as $t \rightarrow 0$. The discontinuous
 4 behaviour along this line is clearly an exchange of dominance between the two saddles.
 5 The superoscillations appear predominantly for $x > 0$ and can definitely be ascribed to the
 6 saddle at x_2 . For $x < 0$ we initiate the wavefunction with superoscillating behaviour, but
 7 this is very quickly suppressed because of the dominance of the saddle at x_4 which does not
 8 display superoscillating behaviour. In the region where the superoscillations occur for $x \leq 0$
 9 the wave pattern cannot be definitively ascribed to either saddle and the minor factors in
 10 equation (19) may be what determines the dominance. To see this we plot the contribution
 11 to the total wave from each saddle at particular times in Figure 10. At very low times Figure
 12 10a shows that for $x < 0$ the contributions from both saddles are of the same order and
 13 run approximately parallel. However one contribution is superoscillating and the other does
 14 not pass through zero in this region. When the contribution from the saddle at x_2 passes
 15 through zero the saddle at x_4 dominates and well away from these zeroes the saddle at x_2
 16 dominates. At slightly later times in Figure 10b the contributions have moved so they are not
 17 quite parallel and the region of space where we cannot definitely ascribe dominance to either
 18 saddle has reduced. For $x \lesssim -0.15$ the saddle at x_4 dominates while for $x \gtrsim 0$ the saddle
 19 at x_2 dominates and leads to superoscillations. For $-0.15 \lesssim x \lesssim 0.0$ neither contribution is
 20 dominant and superoscillations will be terminated in this region at around this time. Figure
 21 10 shows a later time where the contribution from the saddle at x_2 is still superoscillating,
 22 but below $x = 0$ it is completely dominated by the saddle at x_4 so superoscillations are
 23 suppressed in this region. For $x > 0$ it is the saddle at x_2 that dominates, but it does not
 24 super oscillate in this region. Finally we see in Figure 10d a much later time where the
 25 superoscillations no longer occur in the saddle at x_2 and the contribution from the saddle at
 26 x_4 is oscillating more rapidly. Nonetheless, no superoscillations occur at this time regardless
 27 of which saddle point dominates. An interesting point to note is that on close inspection of
 28 figures 10a, b, and c there is a slight discontinuity in the curve due to the saddle point at x_2 .
 29 This is because the the pole at $x' = x + ct$ interferes with this saddle point, $x_2 \rightarrow x + ct$ and
 30 $\phi''(x_j : x, t) \rightarrow \infty$. and the approximation of treating the saddle and the pole separately
 31 becomes incorrect. The effect is surprisingly small. We have used the methods described in
 32 the appendix to treat the case where the saddle point and pole coalesce, but that makes no
 33 difference to our interpretation of our results, so it is not presented here.
 34
 35
 36
 37
 38
 39
 40
 41
 42
 43
 44
 45
 46
 47
 48
 49
 50
 51
 52
 53
 54
 55
 56
 57
 58
 59
 60

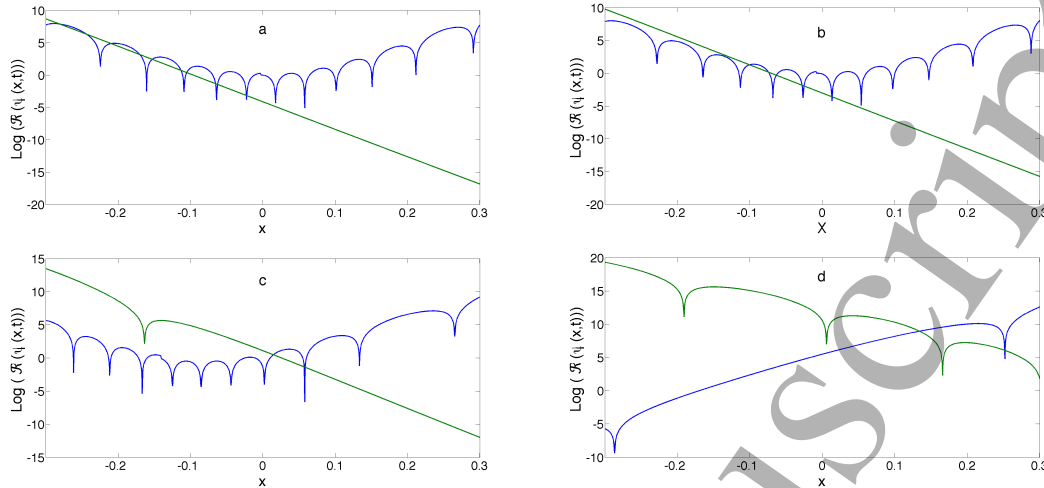


FIG. 10. Superoscillations for the relativistic wavefunction of equation (19) blue line contribution from the saddle point at x_2 , green line contribution from the saddle point at x_4 at: a $t = 0.0005\pi$; b $t = 0.0015\pi$; c $t = 0.025\pi$; d $t = 0.125\pi$

C. Analysis

We have calculated the superoscillations for the wavepacket of equation (1) using the propagator and shown that the evolution of the wavepacket is dominated by contributions from two complex saddles. The superoscillations are associated with the saddle point at x_2 . It is clear from figure 7, 9 and 10 that there is an anti-Stokes line which marks the exchange in dominance of the two saddles. In general therefore superoscillations occur where the saddle at x_2 is dominant and do not occur where the saddle point at x_4 dominates the wavefunction. Here we present a more quantitative approach to this exchange of dominance. As it happens the saddle point x_4 is more or less constant over the the region of small x where our approximations apply. It takes on the value

$$x_4 = -s - \frac{i}{ak}$$

s was originally introduced simply to make the units consistent in our definition of the regional wavepacket. Now we find it has a crucial role in the theory, being the real part of one of the key saddle points. and if we evaluate the wavenumber associated with this saddle it is trivial to see that

$$q_4 = \frac{1}{Ncs} \Re(q(x_4)) = \frac{1}{Ncs} \frac{2ak}{4 + a^2s^2k^2}$$

1
2
3 This means that for our values of the parameters $N = 20$, $a = 4$, $c = 2$ and $k = 1$ the
4 effective wavelength is 40π .(although our approximations are only valid over a small region
5 around $x = 0$).
6
7

8 The saddle point at x_2 is not constant, but can be fit very well with a simple polynomial
9 linear in x and t . While the fit is optimised for this particular values of parameters, com-
10 putational experiments have shown that the fit is satisfactory over a broad range of these
11 parameters. It also turns out that the anti-Stokes line shown in Figure 9 can be fit with a
12 polynomial that is cubic in time and so choosing a value of t enables us to find the associated
13 wavenumber on the anti-Stokes line. At times just greater than $t = 0$ the wavenumber is
14 close to $q_2 = 4$. It decreases rapidly and falls below unity at $t = 0.16$. While these numbers
15 are specific to the wavefunction of equation (1), we expect that an analogous procedure will
16 produce qualitatively similar results for any well-behaved superoscillating wavepacket. Thus
17 we have an understanding of both the wall effect and the life time of the superoscillations.
18
19
20
21
22
23
24
25

26 There are some superoscillations to the left of the anti-Stokes line in figure 9. The reason
27 for this is as follows. As we go from the anti-Stokes line towards $x = -\infty$ at low times
28 the contribution to the wavepacket from both saddles is rising at approximately the same
29 rate. While the contribution from the saddle at x_4 is rising linearly, the contribution from
30 the saddle at x_2 is oscillating rapidly with increasing amplitude. Over a short region of x
31 the minimum in x_2 is more negative than the positive contribution from the x_4 saddle and
32 so the total wavepacket still passes through zero and the superoscillations persist. They
33 have only certainly disappeared when the x_4 contribution is greater than the amplitude of
34 oscillating of the x_2 contribution. So the persistence of the superoscillations to the right of
35 the antiStokes line is a simple two-wave interference effect.
36
37
38
39
40
41
42
43

44 Figure 9 is very different from the corresponding figure of the non-relativistic theory
45 (Figure 6 in reference [23]). In the non-relativistic theory there are both Stokes and anti-
46 Stokes lines that are key, as well as a branch cut and a central point from which all these
47 lines emanate. This has not appeared in the relativistic theory. In fact there is a more
48 complex arrangement of such lines in the relativistic theory as well, but they exist relatively
49 far from the origin and so do not affect the superoscillations at all. As $c \rightarrow \infty$ the poles
50 move off to $x' \rightarrow \pm\infty$ and become completely irrelevant. Also in this limit the real part of
51 the saddle point $x_4 \rightarrow 0$ and then the saddle points can, and do, interfere with each other
52 close to the origin creating a much richer structure of Stokes and anti-Stokes lines in the
53
54
55
56
57
58
59
60

regions close to where the superoscillations occur.

IV. SPIN-1/2 WAVEPACKETS

A. The Dirac Equation

The fundamental equation of relativistic quantum theory is the Dirac equation

$$(i\gamma^\mu \partial_\mu - Nc)\psi(\mathbf{r}, t) = 0 \quad (20)$$

Here we have defined $N = m/\hbar$. The 4×4 γ -matrices can be chosen for convenience provided they obey well known anticommutation relations [27]. We choose the representation suggested in reference [39]

$$\gamma^0 = \begin{pmatrix} 0 & I \\ I & 0 \end{pmatrix} \quad \gamma^i = \begin{pmatrix} 0 & -\sigma^i \\ \sigma^i & 0 \end{pmatrix} \quad (21)$$

Here I is the 2×2 identity matrix and σ^i are the standard Pauli spin matrices. The wavefunction is a four component quantity $(\psi_1(\mathbf{r}, t), \psi_2(\mathbf{r}, t), \psi_3(\mathbf{r}, t), \psi_4(\mathbf{r}, t))^T$. Putting these into equation (20) gives

$$\begin{aligned} \psi_1(\mathbf{r}, t) &= -\frac{i}{Nc} \left[\left(\frac{1}{c} \frac{\partial}{\partial t} + \frac{\partial}{\partial z} \right) \psi_3(\mathbf{r}, t) + \left(\frac{\partial}{\partial x} - i \frac{\partial}{\partial y} \right) \psi_4(\mathbf{r}, t) \right] \\ \psi_2(\mathbf{r}, t) &= -\frac{i}{Nc} \left[\left(\frac{1}{c} \frac{\partial}{\partial t} - \frac{\partial}{\partial z} \right) \psi_4(\mathbf{r}, t) + \left(\frac{\partial}{\partial x} + i \frac{\partial}{\partial y} \right) \psi_3(\mathbf{r}, t) \right] \\ \psi_3(\mathbf{r}, t) &= -\frac{i}{Nc} \left[\left(\frac{1}{c} \frac{\partial}{\partial t} - \frac{\partial}{\partial z} \right) \psi_1(\mathbf{r}, t) - \left(\frac{\partial}{\partial x} - i \frac{\partial}{\partial y} \right) \psi_2(\mathbf{r}, t) \right] \\ \psi_4(\mathbf{r}, t) &= -\frac{i}{Nc} \left[\left(\frac{1}{c} \frac{\partial}{\partial t} + \frac{\partial}{\partial z} \right) \psi_2(\mathbf{r}, t) - \left(\frac{\partial}{\partial x} + i \frac{\partial}{\partial y} \right) \psi_1(\mathbf{r}, t) \right] \end{aligned} \quad (22)$$

These equations define the relations between the different components of the Dirac wavefunction. It is well-known that if we eliminate components between them each individual component obeys the Klein-Gordon equation. We will make use of this fact in what follows.

Now we are going to specialise down to 1+1 dimensions. Firstly let us consider motion confined to the z -axis. Then these equations become

$$\psi_1(z, t) = -\frac{i}{Nc} \left(\frac{1}{c} \frac{\partial}{\partial t} + \frac{\partial}{\partial z} \right) \psi_3(z, t)$$

$$\begin{aligned}
\psi_2(z, t) &= -\frac{i}{Nc} \left(\frac{1}{c} \frac{\partial}{\partial t} - \frac{\partial}{\partial z} \right) \psi_4(z, t) \\
\psi_3(z, t) &= -\frac{i}{Nc} \left(\frac{1}{c} \frac{\partial}{\partial t} - \frac{\partial}{\partial z} \right) \psi_1(z, t) \\
\psi_4(z, t) &= -\frac{i}{Nc} \left(\frac{1}{c} \frac{\partial}{\partial t} + \frac{\partial}{\partial z} \right) \psi_2(z, t)
\end{aligned} \tag{23}$$

As expected the Dirac equation has separated into two identical pairs, one pair representing a spin up particle and the other pair a spin down particle. This tells us that superoscillations in a spin-up particle will be identical to those in a spin-down particle. As these equations are identical we need only consider one of them.

Let us look at what happens if we consider motion confined to the x -axis. To proceed we are going to set $\psi_2(\mathbf{r}, t) = 0$. This means we do not have the most general solution of the Dirac equation. Putting this into the equations for $\psi_3(\mathbf{r}, t)$ and $\psi_4(\mathbf{r}, t)$ and substituting these back into the expression for $\psi_2(\mathbf{r}, t)$ gives zero identically, so this procedure is valid.

In that case

$$\begin{aligned}
\psi_1(x, t) &= -\frac{i}{Nc} \left(\frac{1}{c} \frac{\partial \psi_3(x, t)}{\partial t} + \frac{\partial \psi_4(x, t)}{\partial x} \right) \\
\psi_3(x, t) &= -\frac{i}{Nc^2} \frac{\partial \psi_1(x, t)}{\partial t} \\
\psi_4(x, t) &= \frac{i}{Nc} \frac{\partial \psi_1(x, t)}{\partial x}
\end{aligned} \tag{24}$$

With these limitations we can also put the expressions for $\psi_3(x, t)$ and $\psi_4(x, t)$ into the expression for $\psi_1(x, t)$ to obtain the Klein-Gordon equation (5) [27, 40] for $\psi_1(x, t)$ as expected. Now it is easy to find the solution of the Dirac equation for these cases. For motion in the z -direction we take a solution of the one-dimensional Klein-Gordon equation and differentiate it with respect to z and time to determine $\psi_3(z, t)$ in equation (23). For motion in the x -direction we also take a solution of the one-dimensional Klein-Gordon equation and differentiate it with respect to t and x to determine $\psi_3(x, t)$ and $\psi_4(x, t)$ respectively in equation (24).

The procedure required to investigate superoscillations in a Dirac wavepacket is now clear. $\psi_1(\mathbf{r}, t)$ is set up as a solution of the Klein-Gordon equation starting from the initial wavefunction of equation (1) in its representation as a Fourier series. Then we can use

the procedure above to find the other components of the wavefunction. We have done this and the results are shown in Figure 11. Figure 11a shows the large component of the wavefunction. By construction this is identical to the superoscillations in the Klein-Gordon equation shown in figure 4b. It is independent of the direction of motion. In figure 11b we see the superoscillations in the small component of the wavepacket assuming the momentum is parallel to the spin. i.e. the small component is calculated using the third of equations (23). Figures 11c and d show the superoscillations in the small components of the wavepacket assuming the spin is perpendicular to the momentum. These are deduced from the third and fourth of equations (24).

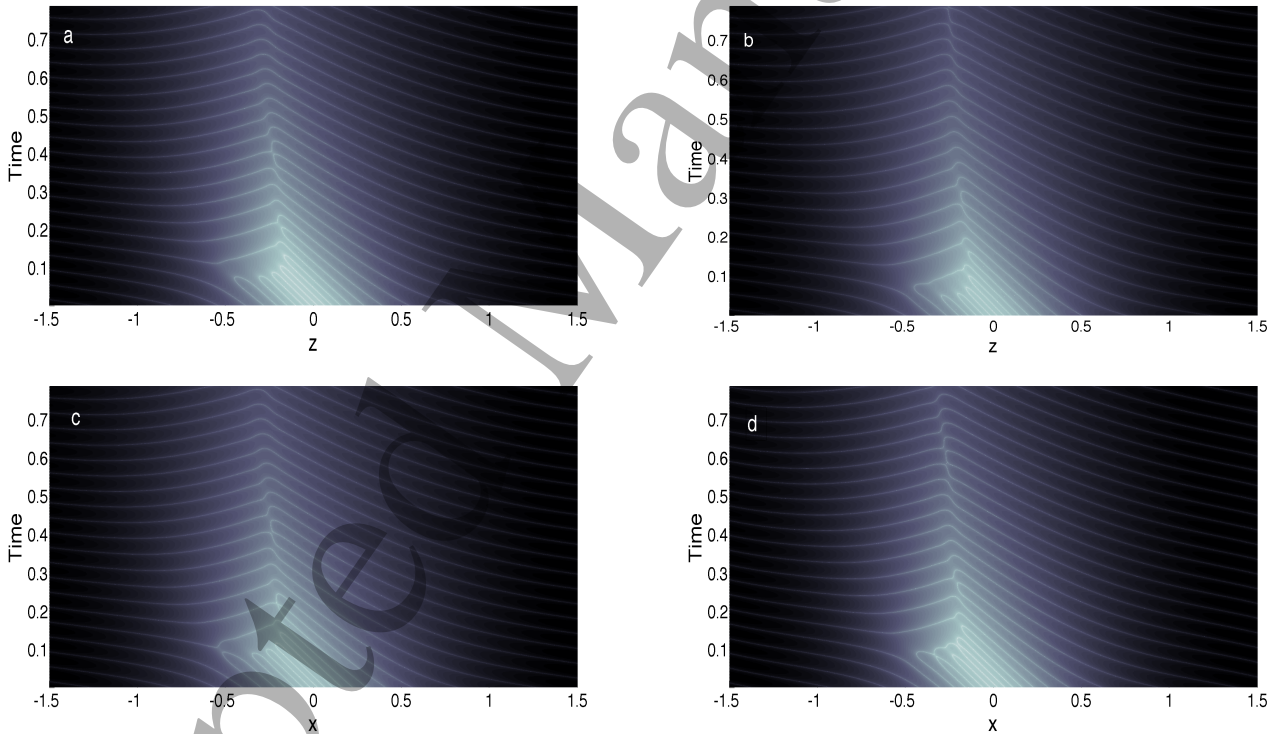


FIG. 11. Space time map of superoscillations from the Dirac equation. a. in $\psi_1(\mathbf{r}, t)$, the large component of the wavefunction. This is independent of whether the motion is in the x or z directions; b. in $\psi_3(z, t)$, the small component of the wavepacket when the momentum is parallel to the spin, c. $\psi_3(x, t)$, one of the small components of the wave-packet when the momentum is perpendicular to the spin; and d. in $\psi_4(x, t)$, the extra small component of the wavefunction when the momentum is perpendicular to the spin.

B. Analysis

The large component of the wavefunction is a solution of the Klein-Gordon equation and the superoscillations shown in Figure 11a have the same origin as previously. It is well described by equation (19) which describes the full wavefunction as a sum of contributions from two saddle points. The superoscillations evolve from the saddle point at x_2 . The wall effect originates from the exchange of dominance between the two saddle points as described earlier. The anti-Stokes line separating these two regions is clearly visible. We can carry this description of $\psi_1(\mathbf{r}, t)$ through to equations (23) and (24) and differentiate the contribution from each saddle point separately, then add them to get the full contribution for each small component of the wave-packet. If we do this the separate regions where the saddle points dominate and the anti-Stokes line should remain the same and indeed in Figure 11b, c and d this is apparent. The general solution of the Klein-Gordon equation is given by equation (6) and to obtain the other components of the solution of the Dirac equation in this representation only requires some differentiations (that was the reason for this particular choice of the gamma-matrices) which do not change the exponentials in the wave-packet, so the saddle points will be the same for all components of the wavefunction. This means we will also observe the same wall effect and lifetime.

The superoscillations in the Dirac case are essentially unobservable because they are exponentially small and because when one component of the wavefunction passes through zero the other components cannot be zero and that means the probability density is always greater than zero in a single particle theory. This means the superoscillations are superimposed on a finite density and cannot be observed using logarithms as done for the individual components of the wave-packet.

V. CONCLUSIONS

The Klein-Gordon equation is a relativistic single particle equation representing spin-0 particles. Evolution of an initially superoscillating wavepacket demonstrates that the superoscillations decay and exhibit a wall effect similar to that of the non-relativistic theory [23]. These can be understood in terms of the dominance of different saddle point contributions to the wavepacket. Because of the existence of the negative energy states in relativistic

theory the number of saddle points is four rather than the two of the non-relativistic theory. This means that there is no simple expression for the saddle points as there is in the non-relativistic case and so we are more reliant on numerical work here. Although the arrangement of Stokes and anti-Stokes lines are very different in the region of space-time where superoscillations exist in the non-relativistic and relativistic theories, the decay of superoscillations and the wall effect have the same origin in both cases. There are differences in detail, but in both cases the wall effect and the lifetime of the superoscillations can be understood in terms of the interaction of contributions from different saddle points with strongly differing wavenumbers to the wavepacket. The key difference between the relativistic and non-relativistic theories turns out to be the position of the (nearly) constant saddle point. In the non-relativistic theory it has real part zero and this means there are Stokes lines and a branch cut which all have to be considered because they all lie in the region of space-time in which superoscillations occur. In the relativistic theory this saddle point has been lifted above zero and away from the region where superoscillations occur. Then the Stokes line and branch cut are also not in the superoscillating region of space-time and so need not be considered. This is true for both spin-0 and spin-1/2 wave-packets.

Berry and Popescu[23] pointed out that one way to explore the evolution of superoscillations experimentally could be to exploit the periodicity of $\psi(x)$ as a representation of a diffraction grating. Such a grating will transform incident particles into a series of diffracted beams. They have shown how this occurs and produced density plots of waves beyond the diffraction grating in their figure 8 which show super oscillatory fine structure for light on a scale of $\lambda/4$. They were able to compare the paraxial and exact fields and found substantial differences in detail, but not sufficient to affect their conclusions. The paraxial wave equation is mathematically identical to the Schrödinger equation, so the non-relativistic limit of our work should look identical to the paraxial limit of theirs, and indeed it does. We use their parameters $N = 10$ and $a = 8$ and set $c = 50$ and then we are able to reproduce their figures 8a and c exactly to the limit of the resolution of their figures. As we reduce c relativistic effects become progressively more emphasised. Therefore a procedure to examine the importance of relativistic effects in superoscillations experimentally would be to do this experiment and then find the optimal value of c to fit the results. Unfortunately, emphasising relativistic effects by decreasing c does not change the scale of superoscillatory behaviour, it remains at about $\lambda/4$. The duration of the superoscillations also remains constant until the strongly

relativistic limit when it decreases rapidly. Finally, in common with several other analyses [14, 21, 24–26] we find that the lifetime of the superoscillations in this wavepacket is much the same as that in the non-relativistic case and is, at least approximately, proportional to N .

VI. APPENDIX: THE KLEIN-GORDON PROPAGATOR

The properties of first quantised relativistic propagators are rarely discussed. Therefore in this appendix we provide a brief review of their derivations and approximations. We begin by defining $\Delta(x-x', t)$ which propagates the wavefunction at the point $(x', 0)$ through space-time. To represent the evolution of a full wavepacket we have to sum over all initial points to yield

$$\psi(x, t) = \int_{-\infty}^{\infty} \psi(x', 0) \Delta(x'; x, t) dx'$$

which is the familiar integral definition of a propagator. For $t = 0$ we must have $\Delta(x', x, t) = \delta(x')$. It is a standard calculation [29] to show that

$$\Delta_{\pm}(x', x, t) = \pm \frac{iN}{\pi} c^2 t \frac{K_1(Nc\sqrt{(x-x')^2 - c^2t^2})}{\sqrt{(x-x')^2 - c^2t^2}} \quad (25)$$

Here K_1 is a modified Bessel function [37] and we have replaced m/\hbar by N from the standard form of the propagator, because that is more convenient for our purposes. If we plot equation (25) on the complex plane we find that it has poles on the real axis at $x' = x \pm ct$ and an infinite number of saddle points off the real axis. Equation (25) is the closed form of our free Klein-Gordon propagator for positive (+)/negative(-) energy states. Making the substitution $t \rightarrow -t$ in the case of the positive energy propagator, gives its negative energy counterpart. This affirms the statement that negative energy wavefunctions are positive energy wavefunctions moving backwards in time. Equation (25) is the starting form used in all our calculations. It has been shown by Thaller [29] that equation (25) can be written in a useful alternative form in different regions of space-time

$$\Delta_{\pm}(x'; x, t) = \frac{Nc^2t}{2} \begin{cases} \mp \frac{H_1^{(2)}(Nc\sqrt{c^2t^2 - (x-x')^2})}{\sqrt{c^2t^2 - (x-x')^2}} & (x + ct > x') \\ \frac{2i}{\pi} \frac{K_1(Nc\sqrt{(x-x')^2 - c^2t^2})}{\sqrt{(x-x')^2 - c^2t^2}} & (|x| + ct < |x'|) \\ \pm \frac{H_1^{(1)}(Nc\sqrt{c^2t^2 - (x-x')^2})}{\sqrt{c^2t^2 - (x-x')^2}} & (x - ct < x') \end{cases} \quad (26)$$

A. The Light Cone Approximation

If we assume the major contribution to the wavefunction comes from the contribution at the poles of the propagator, equation (25) can be approximated as follows. The argument of the modified Bessel function can be written [37]

$$\lim_{x' \rightarrow x \pm ct} K_1(Nc\sqrt{(x-x')^2 - c^2t^2}) \approx \frac{1}{Nc\sqrt{(x-x')^2 - c^2t^2}} \quad (27)$$

leading to

$$\Delta_{\pm}(x'; x, t) = \pm \frac{ict}{\pi} ((x-x')^2 - c^2t^2)^{-1} \quad (28)$$

Although we have derived this from equation (25) it can also be found from equation (26) coming to the pole from either side.

B. The Saddle Point Approximation

Dealing with only the poles of the propagator may well not be a sufficiently robust approximation. Therefore we consider the contribution of the saddle points to the integral of equation (10). We are working with $N \gg 0$ which means we can approximate the Bessel function in equation (25) using equation 10.25.3 in reference [37] and the propagator becomes

$$\Delta(x'; x, t) \approx ict \sqrt{\frac{Nc}{2\pi}} \frac{\exp\left[-Nc\sqrt{(x-x')^2 - c^2t^2}\right]}{((x-x')^2 - c^2t^2)^{3/4}} \quad (29)$$

Unlike the light cone approximation, this approach has the unphysical property that the propagator does not become $\delta(x')$ in the limit $(x-x', t) \rightarrow (0, 0)$. The Klein-Gordon propagator shares this disagreement between the light cone limit and the large argument limit with some curved space propagators [38]. Even if Nc is not particularly large this approximation is still a good one when $x-x' \gg ct$, so it can provide insight into the acausal contributions to the wavefunction. Once we have made approximations to the propagator it is important to demonstrate how good they are. To this end we show in figure 12 the exact propagator and both the light cone and the saddle point approximations to it for a series of values of x and t . We can deduce from this that at all times apart from very close to $t = 0$ the saddle point approximation is better than the light cone approximation.

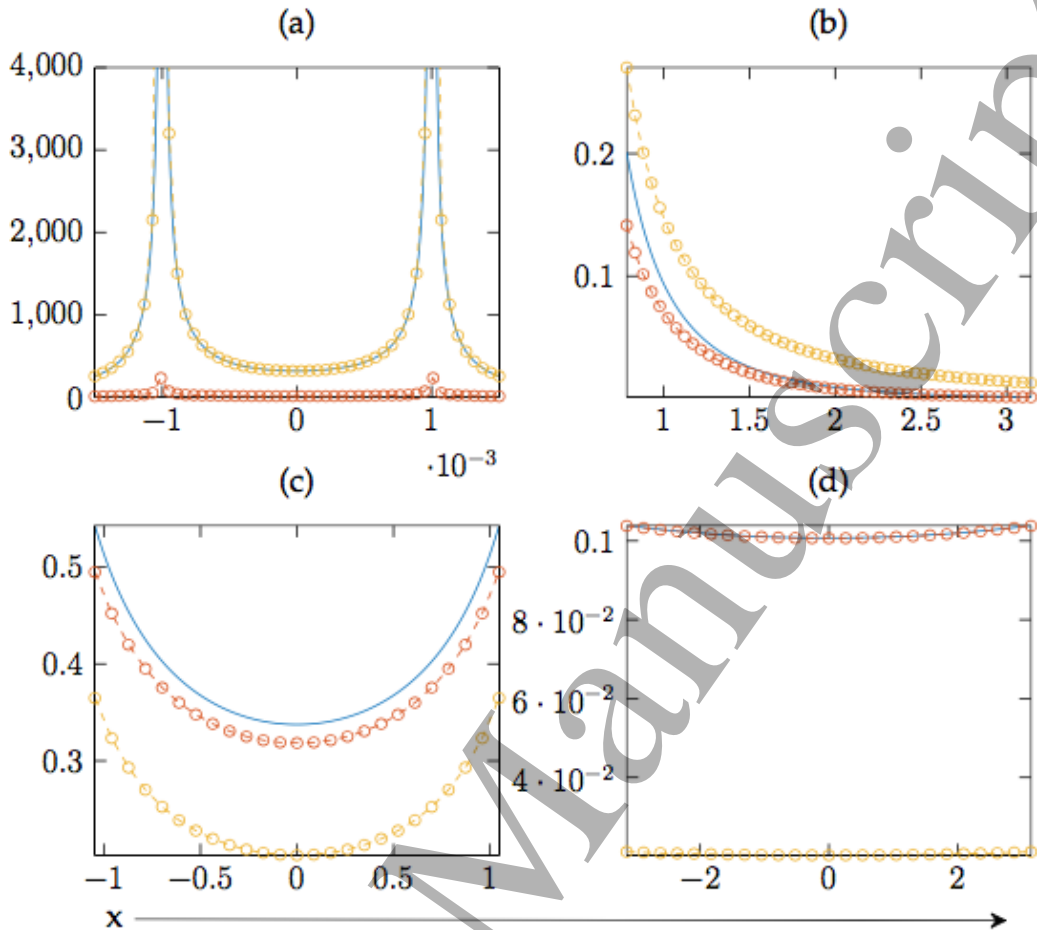


FIG. 12. The exact positive energy Klein-Gordon propagator (25) (blue line), the light cone approximation equation (28) (yellow line) and the WKB approximation (29) (orange line) for (a) $t = 0.001$ and $-0.0015 \leq x \leq +0.0015$; (b) $t = \pi/8$ and $\pi/4 \leq x \leq \pi$; (c) $t = \pi/2$ and $-\pi/3 \leq x \leq \pi/3$; (d) $t = 5\pi$ and $-\pi \leq x \leq \pi$. We have used $x' = 0$ and $m = \hbar = c = 1$.

C. The Saddle-Pole Approximation

The above two sections treat the saddle points and poles separately. This is correct if the saddles and poles are far apart. However that may not always be the case. If they do become close to one another it is not correct to treat them separately. The saddle and pole are said to coalesce when this occurs. Indeed, for our case Figure 6 shows the saddle point x_2 and the pole at $x' = x + ct$ may well coalesce. This is difficult to deal with because the approximations are not equal at the pole, the saddle point approximation has a singularity at this point while the light cone approximation has a simple pole. Therefore we need a new

approximation. To obtain a suitable propagator for this case we employ a Mellin-Barnes representation of the modified Bessel function [37]

$$K_1\left(Nc\sqrt{(x-x')^2-c^2t^2}\right) = \frac{i}{2\pi^2} \left(\frac{\pi}{2Nc\sqrt{(x-x')^2-c^2t^2}}\right)^{1/2} \exp\left(-Nc\sqrt{(x-x')^2-c^2t^2}\right) \times \int_{-i\infty}^{i\infty} \Gamma(\tau)\Gamma\left(-\tau-\frac{1}{2}\right)\Gamma\left(\frac{3}{2}-\tau\right)\left(2Nc\sqrt{(x-x')^2-c^2t^2}\right)^\tau d\tau \quad (30)$$

Substituting this into equation (25) gives

$$\Delta_\pm(x', x, t) = \mp \frac{Nc^2t}{2\pi^3} \left(\frac{\pi}{2Nc\sqrt{(x-x')^2-c^2t^2}}\right)^{1/2} \frac{\exp\left(-Nc\sqrt{(x-x')^2-c^2t^2}\right)}{\sqrt{(x-x')^2-c^2t^2}} \times \int_{-i\infty}^{i\infty} \Gamma(\tau)\Gamma\left(-\tau-\frac{1}{2}\right)\Gamma\left(\frac{3}{2}-\tau\right)\left(2Nc\sqrt{(x-x')^2-c^2t^2}\right)^\tau d\tau \quad (31)$$

We see that the pre-factor here looks very similar to the propagator in the saddle point approximation. The integral in equation (31) can be done by rearranging equation (30). Then using equation (27) for the Bessel function leads to the same expression as we found in the light cone approximation. However in this limit the exponent tends to zero so the exponential can be approximated by unity.

Therefore, in order to have a propagator that is valid when the saddle point and pole coalesce we keep the prefactor as it is but evaluate the integral in the light-cone approximation. Making use of equation (27) a little algebra yields

$$\Delta_\pm(x', x; t) = \mp \frac{ict}{\pi} \frac{1}{(x-x')^2-c^2t^2} \exp\left(-Nc\sqrt{(x-x')^2-c^2t^2}\right) \quad (32)$$

This approximation has the desired properties. As we take the light-cone limit it behaves as a simple pole, whereas moving away from this into the saddle point regime, the exponential takes over. Equation (32) also yields a δ -function as $(x-x', t) \rightarrow (0, 0)$. This expression was obtained as an approximation and it is important to investigate the precision and range of validity of this. In Figure 13 we look at the accuracy of the saddle-pole approximation. As expected this expression does provide improved accuracy when the saddle and pole are very close, but the overall effect can be regarded as small.

In Figure A.2 we look at the accuracy of the saddle-pole approximation. As expected this expression does provide improved accuracy when the saddle and pole are very close, but the overall effect can be regarded as small.

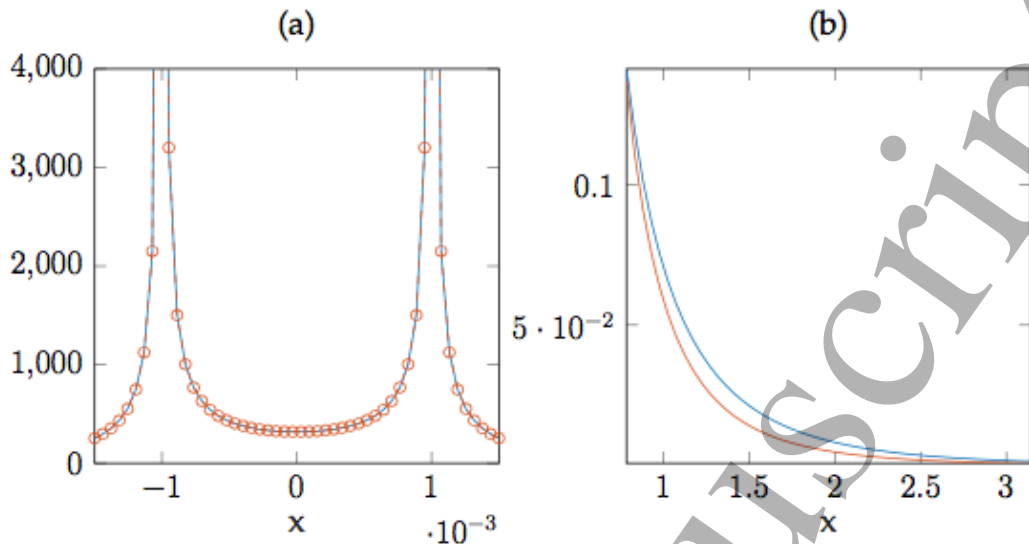


FIG. 13. (a) The exact positive energy Klein-Gordon propagator (25) (blue line), the saddle-pole approximation approximation equation (32) (orange circles) for $t = 0.001$ and $-0.0015 \leq x \leq +0.0015$; (b) The saddle point approximation (29) and the saddle-pole approximation (32) to the propagator for $t = \pi/8$ and $\pi/4 \leq x \leq \pi$.

D. The Non-Relativistic Propagator

In this paper we frequently refer to the non-relativistic limit to relate this work to earlier results. Therefore, for completeness, we examine the non-relativistic limit of equation (25). In this limit $c \rightarrow \infty$, and the argument of the modified Bessel function becomes large. This means we can use equation 10.25.3 of reference [37] to approximate the Bessel function as

$$K_1(Nc\sqrt{(x-x')^2 - c^2t^2}) = \sqrt{\frac{\pi}{2Nc\sqrt{(x-x')^2 - c^2t^2}}} \exp(-Nc\sqrt{(x-x')^2 - c^2t^2})$$

In this limit we can also write

$$\sqrt{(x-x')^2 - c^2t^2} \approx ict \left(1 - \frac{(x-x')^2}{2c^2t^2} \right) \quad (33)$$

Putting this into equation (25) and multiplying out the denominator inside the square root gives two terms: $2imc^2t$ and $m(x-x')^2/it$. At any time greater than zero the first term dominates so we can neglect the second. We also make approximation (33) in the exponent but do not neglect terms there because we are interested in the phase in this work.

$$\Delta_+(x-x', t) \approx \left(\frac{N}{2\pi it} \right) e^{iN(x-x')^2/(2t)} e^{-iNc^2t} \quad (34)$$

This is the familiar Schrodinger free particle propagator with the extra rest mass term in the phase of the wavefunction in the second exponential as expected.

-
- [1] Francia, G. T. di, 1952, *supplemento Al Volume IX, Serie IX Del Nuovo Cimento*, **3**
 - [2] Aharonov Y, Albert D. Z, and Vaidman L, 1988, *Phys. Rev. Lett.* **60** 1351-4.
 - [3] Berry M. V. *Faster than Fourier* in Quantum Coherence and Reality; in celebration of the 60th Birthday of Yakir Aharonov (J S Anandan and J L Safko, eds.) World Scientific, Singapore, pp 55-65, (1994).
 - [4] Aharonov Y, Colombo F, Sabadini I, Struppa D. C, and Tollaksen J, 2011, *J. Phys. A: Math. Theor.* **44** 365304.
 - [5] Kempf A and Ferreira P. J. S. G, 2004, *J. Phys. A: Math. Gen A* **37** 12067-76.
 - [6] Tollaksen J, 2007, *Journal of Physics: Conference series*, **70**, 012016.
 - [7] Berry M. V. and Moiseyev N, 2014 *J. Phys. A: Math. Theor.* **47** 315203.
 - [8] Katsav E, Perlsman E, and Schwartz M, 2017, *J. Phys. A: Math. Theor.* **50** 025001
 - [9] Berry, M V and Dennis, M R, 2009, *J. Phys. A: Math. Theor.* **42** 022003.
 - [10] Berry, M.V. and Fishman, S. 2018, *J. Phys. A: Math. Theor.* **51** 025205.
 - [11] Berry, M V, 2013, Superoscillations, endfire and supergain, in Quantum Theory: a Two-Time Success Story; Yakir Aharonov Festschrift (editors: D Struppa and J Tollaksen) (Springer), 327-336.
 - [12] Berry, M V, 2016, *Milan Journal of Mathematics* **84** 217-230.
 - [13] Dennis M. R, Hamilton A. C, and Courtial J, 2008, *Optics Letters*, **33**, 24, 2976-8.
 - [14] Aharonov Y, Colombo F, Sabadini I, Struppa D. C, and Tollaksen J, 2011, *J. Phys. A: Math. Theor.* **50** 185201.
 - [15] Berry, M V, 2013, *J. Phys. A: Math. Theor* **46**, 205203.
 - [16] Roy T, Rogers E. T. F and Zheludev N. I, *Optics Express* **21**, no 6. 7577-80.
 - [17] Rogers E. T. F, Lindberg J, Roy T, Savo S, Chad J. E, Dennis M. R, Zheludev N. I, 2012, *Nat. Mater.* **11** 432-5.
 - [18] Gazit S, Szameit A, Eldar Y and Segev M, 2009, *Opt. Express* **17** 23920-46 and *Opt. Express* **18** 26631.
 - [19] Shechtman Y, Gazit S, Szameit A, Eldar Y and Segev M, 2010, *Opt. Lett* **35** 1148-50.

- 1
2
3 [20] Yuan G. H, Vezzoli S, Aluzarra C, Rogers E. T. F, Couteau C, Soci C and Zheludev N. I,
4 2016, *Nature: Light: Science and Applications* **5** e16127.
5
6 [21] Berry M. V. *at. al.* 2019, *J.Opt*, **21**, 053002.
7
8 [22] G Chen, Z. Wen and C. Qiu, 2019, *Nature: Light Sci Appl* **8**, 56
9
10 [23] Berry M. V. and Popescu S. 2006 *J. Phys. A: Math. Gen.* **39** 6965-6977.
11
12 [24] Buniy R. V, Colombo F, Sabadini and Struppa D. C, 2014, *J. Math. Phys.* **55** 113511.
13
14 [25] Bussell M and Strange P, 2015, *Eur. J. Phys.* **36**, 065028.
15
16 [26] Colombo F, Gantner J and Struppa D. C, 2017, *J. Math. Phys.* **58**, 092103.
17
18 [27] P. Strange, *Relativistic Quantum Mechanics with applications in condensed matter and atomic*
19 *physics*, (Cambridge University Press), (1998).
20
21 [28] Gradshteyn I. S, and Ryzhik I. M, 2007 *Tables of Integrals, Series and Products*, (Elsevier,
22 San Diego) 3.961.2.
23
24 [29] Thaller B, 1992, *The Dirac Equation*, (Springer-Verlag, Berlin).
25
26 [30] See K. Hira, 2013, *Eur. J. Phys.* **34**, 777, for example.
27
28 [31] E. T. Copson, *Asymptotic Expansions* (Cambridge University Press, 2005).
29
30 [32] N. G. de Bruijn, *Asymptotic Methods in Analysis*, (Dover, New York) (1981).
31
32 [33] M. V. Berry and M. R. Dennis, 2009, *J.Phys. A: Math. Gen.* **42** 022003.
33
34 [34] M. V. Berry, 2013, *J.Phys. A: Math. Gen.* **46** 205203.
35
36 [35] M. V. Berry and M. Molseyev, 2014, *J.Phys. A: Math. Gen.* **47** 315203.
37
38 [36] M. V. Berry in "Asymptotics beyond all orders" eds H. Segur and S. Tanveer (Plenum, New
39 York). 1-14, (1991).
40
41 [37] NIST 2010, *NIST Handbook of Mathematical Functions*, <http://dlmf.nist.gov>: Cambridge
42 University Press.
43
44 [38] L. S. Schulman, 1981, *Techniques and Applications of Path Integration*, (Wiley, New York).
45
46 [39] I. Bialynicki-Birula and Z. Bialynicki-Birula, 2017, *Phys. Rev. Lett.* **60** 114801,1-5.
47
48 [40] M. V. Berry, 2012, *Eur. J. Phys.* **33**, 279.
49
50
51
52
53
54
55
56
57
58
59
60